

Physical Simulation of Water Inrush through the Mine Floor from a Confined Aquifer

Baohua Guo^{1,2,3}  · Tan Cheng¹ · Long Wang⁴ · Tao Luo¹ · Xiaoyu Yang⁵

Received: 15 January 2017 / Accepted: 28 August 2017 / Published online: 30 August 2017
© Springer-Verlag GmbH Germany 2017

Abstract A physical simulation test system was designed to study the mechanism of water inrush through the mine floor. The results showed that vertical stress in the floor first increased as the mining face approached, then decreased after the face had passed, and finally returned to near its original state as the mine roof falls. At about the same time, the floor first experienced compression as the mining face approached, then heaving after the face had passed, and finally recompression to a position that was a little higher than its original height. Water inrush occurred before the first weighting of the roof but there were no subsequent water inrushes.

Keywords Coal mining · Groundwater hazard · Vertical stress and displacement · Orthogonal test

Introduction

Water inrush through the coal seam floor seriously affects the safe production of coal. There have been 937 such accidents in China's coal mines, resulting in 3887 deaths since fully-mechanized coal mining technology was widely introduced in 2002 (Table 1, after Sun et al. 2016). Scholars have not yet formed a clear and unified understanding of this type of water inrush.

To simulate the water inrush process through a coal seam floor, Guo (2008) and Cheng et al. (2016) analyzed the influences of mining height, water pressure, aquiclude thickness, and excavation distance, and found that water inrush occurred most readily at the open-off cut or mining face. The open-off cut refers to the first roadway that connects the tailgate and headgate, forming a preliminary ventilation system. Yang and Li (1997) found that the fault properties and the size of the gob area were closely related to water inrush from a fault. By establishing physical and numerical models, Wang and Park (2003) decided that the final fracture depth in floor strata primarily depended on the geological and hydraulic conditions, while mining conditions were of secondary importance. Subsequently, the coupling model of rock pressure and seepage was established to study the mechanism of an inrush through the coal floor (Huang et al. 2012). Based on the elastic damage theory, Zhu and Wei (2011) researched the effect of fault structure and karst collapse column on such an inrush. Sun et al. (2015) developed a new kind of similar material applicable for water inrush simulation to reveal the failure characteristics of similar material and the evolution characteristics of water inrush channels. Li et al. (2016) simulated the distribution of stresses and the extent of plastic zones in the floor strata and found that 80% of the total stress caused by water pressure acted on the water side of the first tapered plug and that the magnitude of this total stress gradually decreased along the axial direction of the chamber behind the seal. Yin et al. (2016)

✉ Baohua Guo
guobaohua@139.com

¹ School of Energy Science and Engineering, Henan Polytechnic University, Jiaozuo 454000, China

² Collaborative Innovation Center of Coal Work Safety, Jiaozuo 454000, China

³ Key Laboratory of Safety and High-efficiency Coal Mining, Ministry of Education (Anhui University of Science and Technology), Huainan 232001, China

⁴ School of Safety Science and Engineering, Henan Polytechnic University, Jiaozuo 454000, China

⁵ Shendong Coal Group Company, China Shenhua Energy Company Limited, Dongsheng 017000, China

Table 1 Water inrush accidents in China's coal mines from 2002 to 2016 based on data from China's State Administration of Coal Mine Safety (updated from Sun et al. 2016)

Year	Coal produced (10×10^6 t)	Fatality rate per million tons of production	No. of water inrush accidents	No. of deaths	Accidents with 10 or more victims		Accidents with 30 or more victims	
					No. of accidents	No. of deaths	No. of accidents	No. of deaths
2002	14.1	0.36	159	509	9	130	–	–
2003	17.3	0.32	137	551	14	231	1	35
2004	20	0.18	118	357	5	107	1	36
2005	21.5	0.28	109	605	13	357	3	193
2006	23.3	0.18	99	417	5	124	1	56
2007	25.2	0.10	63	255	3	56	–	–
2008	27.2	0.10	59	263	8	135	1	36
2009	26.2	0.06	47	166	4	54	–	–
2010	32.5	0.07	38	224	6	137	2	70
2011	35.2	0.05	44	192	6	85	–	–
2012	36.6	0.03	24	122	5	57	–	–
2013	37	0.02	21	89	2	28	–	–
2014	38.7	0.02	8	60	1	22	–	–
2015	37.5	0.01	7	41	1	21	–	–
2016	33.6	0.01	4	36	2	24	–	–
Total	425.9	0.09	937	3887	84	1568	9	426

developed a numerical simulation model to describe flood water pathways during mining, and found that ground stress, groundwater pressure, excavation length, working face width, mechanical properties of aquitards, and expansion of fractures by groundwater infiltration all contributed to an inrush.

In geotechnical engineering, the selection of similar materials and associated experimental methods are relatively mature for studying the stability of roadway or mining workspaces. However, few investigations have been successfully carried out on inrushes through the floor. To physically simulate such an inrush, both the confined aquifer and the aquiclude are key factors. A water bag has been used to simulate the confined aquifer below the floor (Li et al. 1997; Zhu et al. 1999), but this does not simulate water flowing through mining-induced fractures after floor breakage. Considering the seepage-stress coupling effects, a test system was designed based on a Chinese-manufactured YDM-E physical mining model test device to study the inrush mechanism of the No. 15031 panel at the Jiulishan coal mine, China.

Design and Establishment of Physical Simulation Test

Geological and Hydrogeological Conditions at the No. 15031 Panel

The Jiulishan coal mine, which is located in the Jiaozuo coalfield of northern Henan province, has been mined for

more than 30 years (Fig. 1a). The maximum and average water inflows of the Jiulishan mine are 6240 and 4800 m³/h respectively. There have been 65 water inrush accidents and 84% of them occurred through the floor. The No. 15031 panel was the prototype for this study (Fig. 1b); its absolute elevation ranges from –294.9 to –324.6 m and it is about 400 m below the ground surface. The strike length is 321 m, the dip width is 110 m, and it spans about 35,310 m². The No. 2-1 coal seam, which dips at an angle of 12°30' is one of the mine's major coal seams; its thickness ranges from 1.5 to 6.5 m. There are three Upper Carboniferous Taiyuan formation limestone aquifers (L8, L91, and L92) under the No. 2-1 coal seam from low to high, and they are separated by an 8.5 m thick siltstone and 2.0 m thick mudstone aquicludes (Fig. 2). The 8.4 m thick L8 limestone, with an in situ permeability coefficient of 0.0036–0.648 m/day and a water pressure of 4.0 MPa, is the main hazard to safe mining of the No. 2-1 seam.

Similar Materials and Proportion Number

According to the rules of physical simulation (Hu et al. 2007a), a physical model was established based on the geological and mining conditions of the No. 15031 panel at Jiulishan coal mine. The ratios between the experimental and prototype models were: the geometric ratio $\alpha_l = 1:100$, the bulk density ratio $\alpha_\gamma = 1:1.6$, the time ratio $\alpha_t = 1:10$, and the stress, strength, and water pressure ratio $\alpha_\sigma = \sigma_p = \alpha_l \alpha_\gamma = 1:160$.

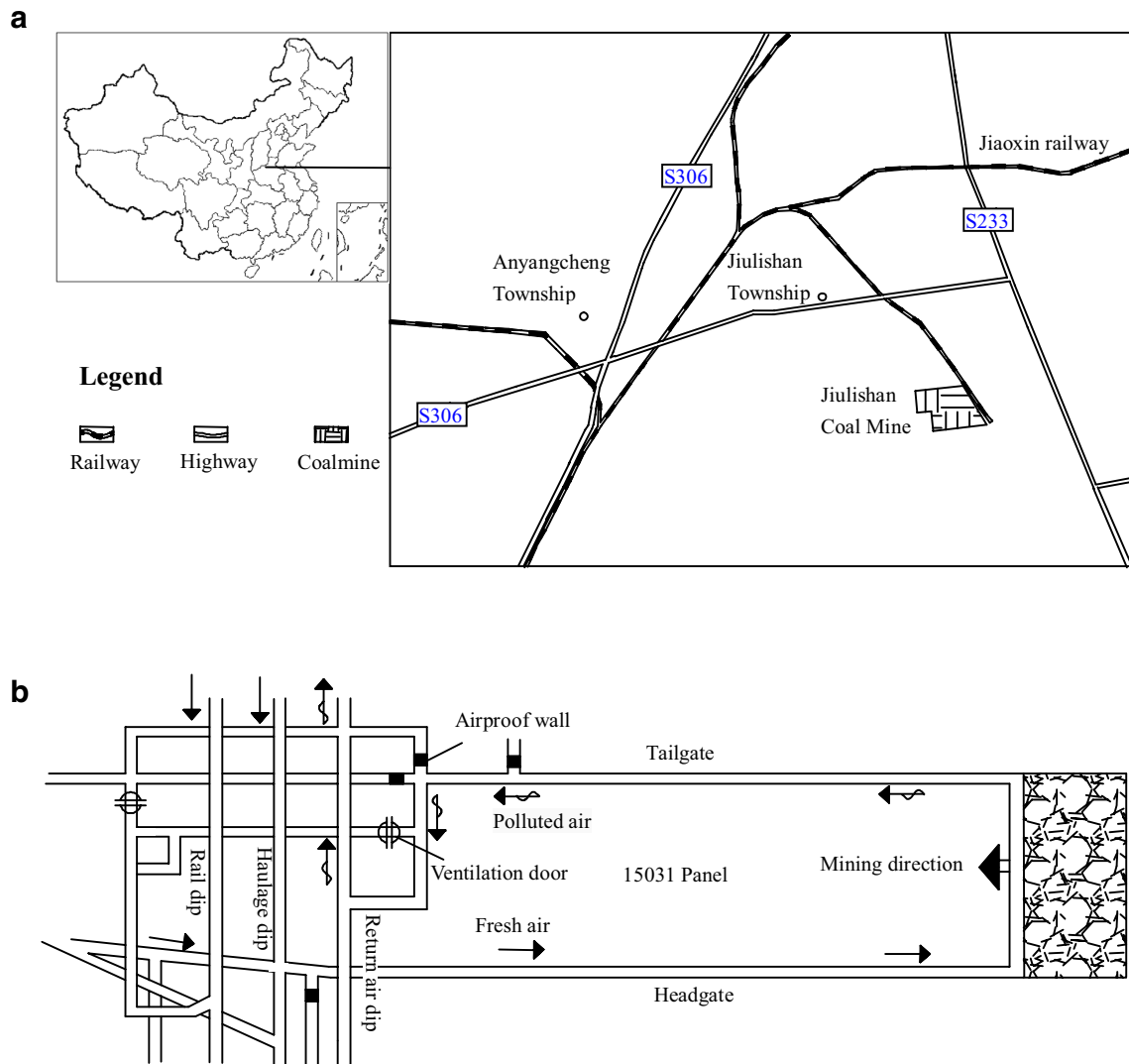


Fig. 1 Engineering site. **a** Location of Jiulishan coal mine; **b** the layout of No. 15031 Panel

In the physical simulation test, pebbles and red clay were respectively used to simulate the aquifer and the main aquiclude (Hu et al. 2007b). Sand, gypsum, calcium carbonate, and borax were used to form the other strata; the calcium carbonate and gypsum were cement materials and a borax solution was used as a retarder to make the initial setting time of the mixing material $\approx 15\text{--}20$ min. Thus, the strengths of the strata were mainly determined by three factors: the sand-cement ratio, calcium carbonate-gypsum ratio, and quality ratio of a 1% borax solution with other solid materials (which is simplified hereafter as the borax solution ratio).

The appropriate proportions of similar materials were experimentally studied using an orthogonal design method for the mechanical aspects of each analogous stratum meeting the correct physicality ratio. Three levels were set for each of the three factors, and an L9 (3^4) orthogonal table was selected (Table 2). Thus, nine mixing ratio tests were

conducted for each rock stratum since the fourth column in L9 (3^4) orthogonal table was removed. Three specimens of the same size ($100\text{ mm} \times 100\text{ mm} \times 100\text{ mm}$) were made of sand, calcium carbonate, gypsum, and borax solution and then uniaxial compression tests were conducted to obtain their average uniaxial compressive strength. Consequently, the proportional numbers of the coal seam, siltstone, and sandstone in the physical simulation model were determined (Table 3), in which the proportion number xyz means that the sand-cement ratio is $x/1$ and the calcium carbonate-gypsum ratio is y/z in cement materials.

Physical Model

The YDM-E mining physical model test device (Fig. 3a, b) was used in the physical simulation, which comprised a loading frame, pneumatic hydraulic test console, simulation

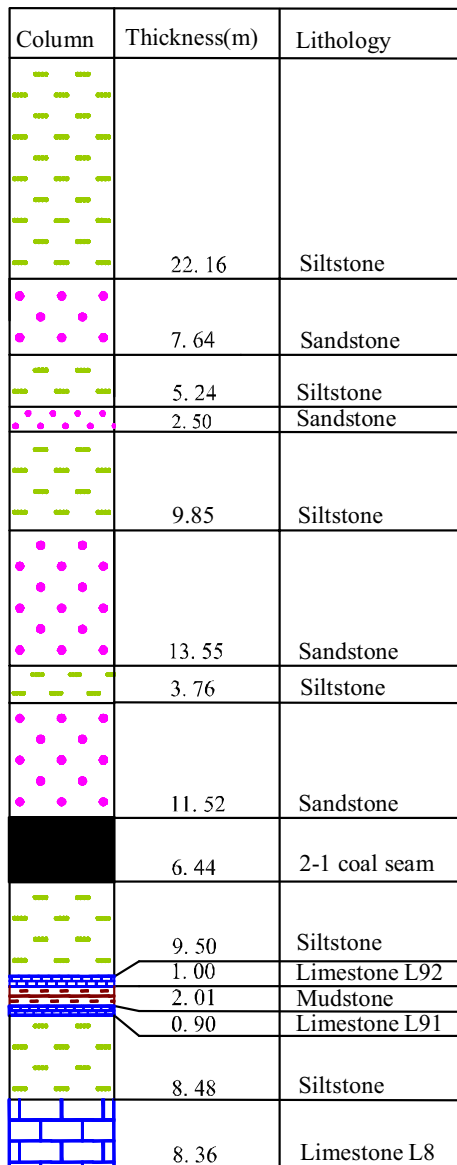


Fig. 2 The borehole histogram of the No. 15031 panel

Table 2 Factors and levels in orthogonal table

Rock stratum	Level	Sand-cement ratio	Calcium carbonate-gypsum ratio	Borax solution ratio
Sandstone	1	5:1	2:8	1/8
	2	6:1	3:7	1/9
	3	7:1	4:6	1/10
Siltstone	1	6:1	4:6	1/8
	2	7:1	5:5	1/9
	3	8:1	6:4	1/10
Coal	1	7:1	6:4	1/8
	2	8:1	7:3	1/9
	3	9:1	8:2	1/10

model (Fig. 3c), a water supply system, and measuring devices. The model was 1600 mm in length, 400 mm in width, and 1600 mm in height and contained four simulated rock layers: overburden strata, the coal seam, an aquitard floor strata, and the confined aquifer. Large-scale geologic structures (such as faults or karst collapse columns) were not considered. The bottom boundary of this model was constrained in the vertical direction, and both the left and right boundaries were constrained in the horizontal direction. A compressive vertical stress of 0.063 MPa was imposed on the top boundary to represent the ground stress induced by the overburden strata. Excavation of the coal seam started at a point 30 cm from the left boundary of the model, as the mining face advanced toward the right. A stepwise excavation method; each step involved an excavation distance of 5 cm to reflect an actual mining advance of 5 m. After each step, 2.5 h was allocated for the surrounding rock to relieve stress and reach a new stress equilibrium state. A total of 39 observation points on three observation lines were arranged in floor between the coal seam and the aquifer to observe the displacement and stress distribution in the excavation process (Fig. 3c), in which observation lines 1–3 were located at depths of 1, 5, and 11.51 cm below the coal seam, respectively. The stress was measured using a BX120-5AA strain gage and the DH3818 static strain test system (Fig. 3a); displacement measurements were conducted using the NTS-362R total station instrument.

The water supply system (Fig. 4) connected the high water tank to the simulated aquifer. A plastic pipe at the bottom of the trough had one closed end; the other, which extended out from the model, was connected to the supply hose, which was supplied from the high water tank. Holes were drilled equidistantly along the pipe inside the trough so that water could flow out freely along the full length of the pipe in the trough. The water level in the tank could be changed to supply different water heads. Additionally, a pipe continually resupplied water into the high water tank and a pipe connecting the higher and lower tanks was used to maintain a constant water table in the high water tank. The height difference between the high water tank and the aquifer was set as 2.5 m to provide 0.025 MPa of water pressure in

Table 3 Proportion of rock strata in the model

Strata	UCS of prototype, MPa	UCS of model, kPa	Proportion (xyz)	Borax solution ratio	Material
Sandstone	54.48	340.50	646	1/10	
Siltstone	37.50	234.38	764	1/8	
Coal seam	12.54	78.40	982	1/10	
Mudstone	28.26	176.60	–	–	Red clay
Limestone	53.40	333.75	–	–	Pebbles

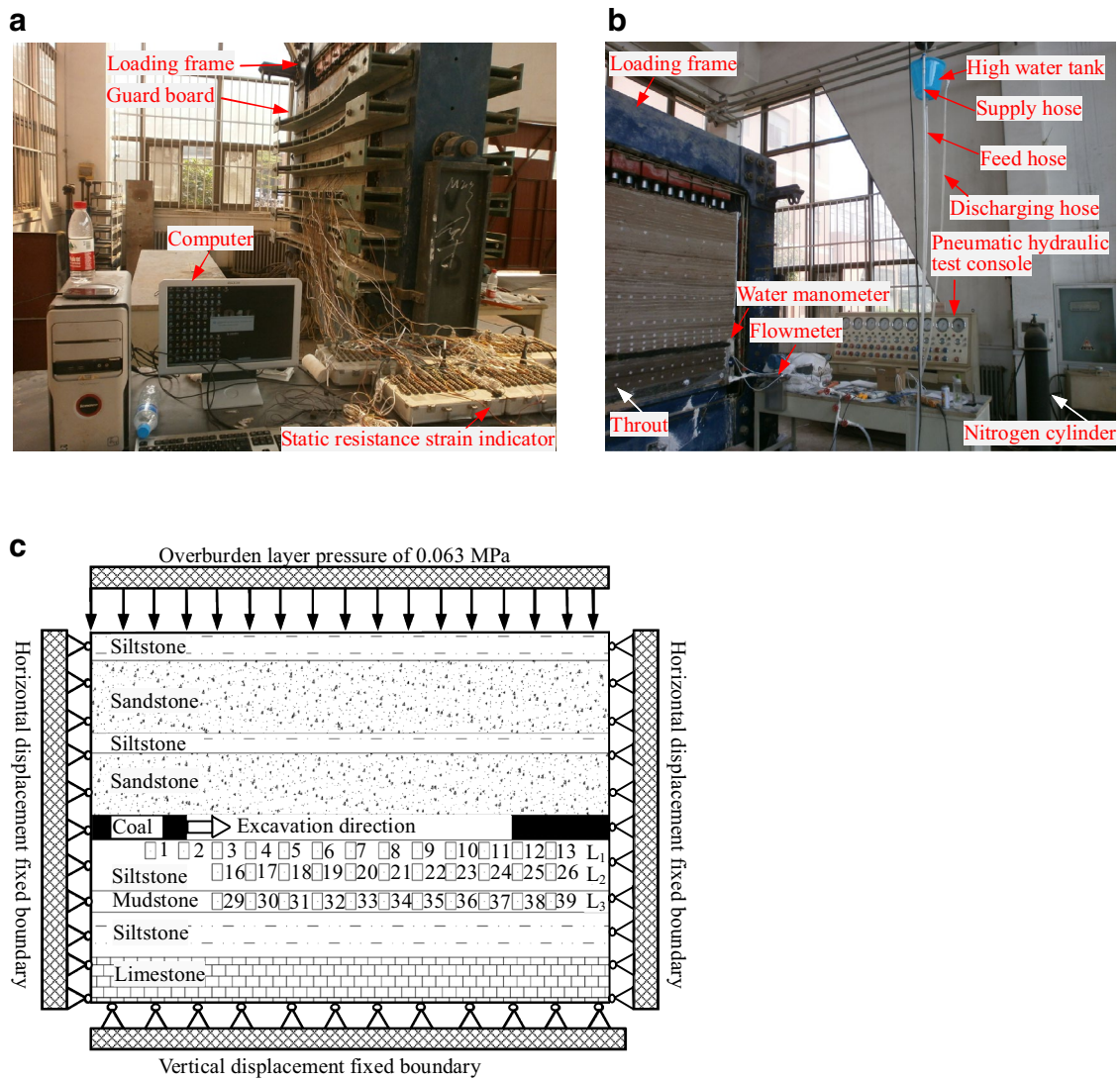


Fig. 3 The YDM-E mining physical model test device: **a** before the guard board is removed; **b** after the guard board is removed; **c** diagram of the physical simulation model

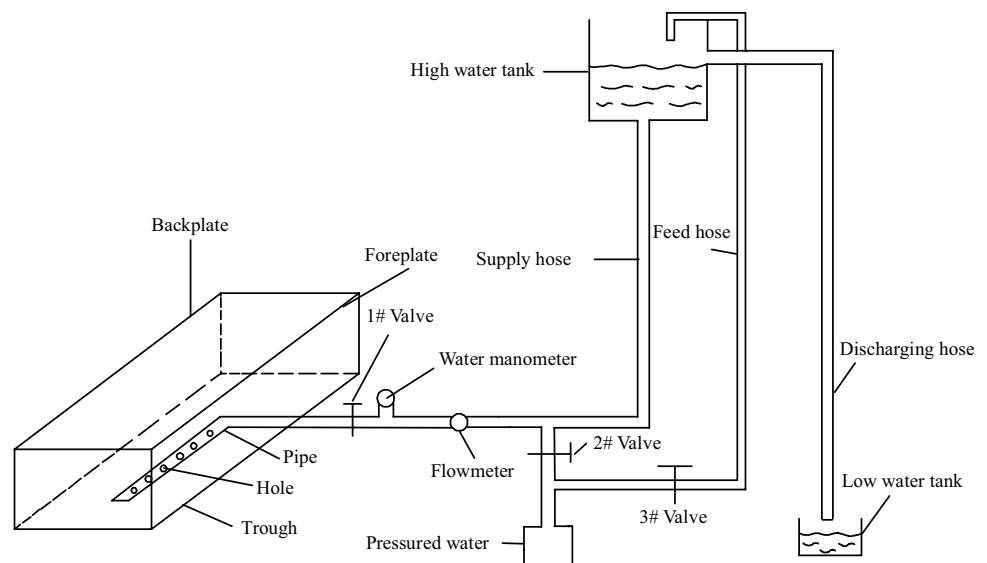
this test. A digital water manometer, mass flow meter, and a paperless recorder were used to monitor water pressure and flow rate, respectively.

The trough was made of transparent Plexiglas with a height equal to the total floor strata below the coal seam. The trough was used to store the aquifer water and prevent it from flowing out through the four sides and the bottom boundary. Both the foreplate and backplate of the trough had to bear the lateral loads, so the plexiglas plates were 2 cm thick; two rows of iron wires were used to laterally fix the foreplate and backplate. Vent holes were designed to exhaust the air in the aquifer when water was supplied into the trough before coal excavation. These vent holes were sealed with a waterproof material when the air in the aquifer was exhausted and water filled the entire aquifer. Additionally, under the

common pressure of the weight of the similar material and upper loads, red clay laterally expands to closely contact the plexiglas plates and help prevent water in the pebble layer from flowing out through the gap between the test materials and plexiglas plates.

Test Results

Vertical stress present in the coal seam floor before excavation will redistribute after excavation, while the vertical displacement in the coal seam floor will experience a corresponding evolution. Figure 5 depicts this vertical stress and displacement in the floor. Because water inrush is directly

Fig. 4 The water supply system

related with the floor, the displacement and stress change law in the roof is no longer analyzed here.

Vertical Stress Evolution in the Floor Strata

The mining-induced stress redistribution that governs the fracturing and water flow in the floor strata is focused on here. The stress-relaxation zone in the floor strata was concentrated largely under the mined-out area, whereas the pressurized zone was located mainly under the coal body around the mined-out area. This is caused by the transfer of the weight of the overburden roof strata in the excavated area to the surrounding coal body. We can see from Fig. 5a–c that the vertical stresses at each measuring point experienced three stages, first increasing as the mining face approached, then decreasing after the face had passed, and finally stabilizing at nearly its original state as the roof fell. The maximum measured vertical stress at the same distance from the open-off cut on observation lines 1–3 sequentially fell during the increasing period, and their minimum vertical stress sequentially increased during the decreasing period. Especially for measuring point 3, which was 12.5 cm from the open-off cut on observation line 1, the vertical stress was at its maximum when the excavation distance reached 10 cm. It then decreased to its minimum value when the excavation distance reached 20 cm and finally returned nearly to its original state when the excavation distance reached about 50 cm. It is apparent that the stressed region ahead of the mining face kept moving forward as the mining face advanced. For measuring points 7 and 11, which were 52.5 and 92.5 cm from the open-off cut, respectively, on observation line 1, the vertical stresses began to be influenced by excavation about 20 cm ahead of the mining face.

Vertical Displacement Evolution of Observation Points in the Floor Strata

The floor strata under the mined-out area will be in a transition state from compression to extension near the mining face, which will inevitably reduce the inherent stability of the rock strata and induce fractures. Fracture development in floor strata during mining is very important when mining above aquifers. The development of cracks in floor strata could not be observed in the test because the materials were not visible; however, it could be assumed by the vertical displacement of the floor strata.

The vertical displacement on observation lines 1–3 changed with increasing excavation distance (Fig. 5d–f). The floor first compressed as the mining face approached, then heaved after the face had passed, and finally gradually recompressed as the roof fell. After that, the vertical displacement in the floor remained roughly constant at an elevation that was a little above its original height. The maximum vertical compression at measurement points that were the same distance from the open-off cut on observation lines 1–3 sequentially decreased during the compressing period, while their maximum heave sequentially decreased in the heaving period. At measuring point 3, which was 12.5 cm from the open-off cut on observation line 1, the compression increased to its maximum value when the excavation distance reached 10 cm, while its heave increased to its maximum value when the excavation distance reached 30 cm and finally it was recompressed roughly to a constant value that was a little above the original height when the excavation distance reached about 50 cm. When the excavation distance reached 30 cm, the heave of the measuring points 3, 16, and 29, which were all 12.5 cm from the open-off cut were 1.47, 1.03, and 0.096 cm, respectively and excavation-induced

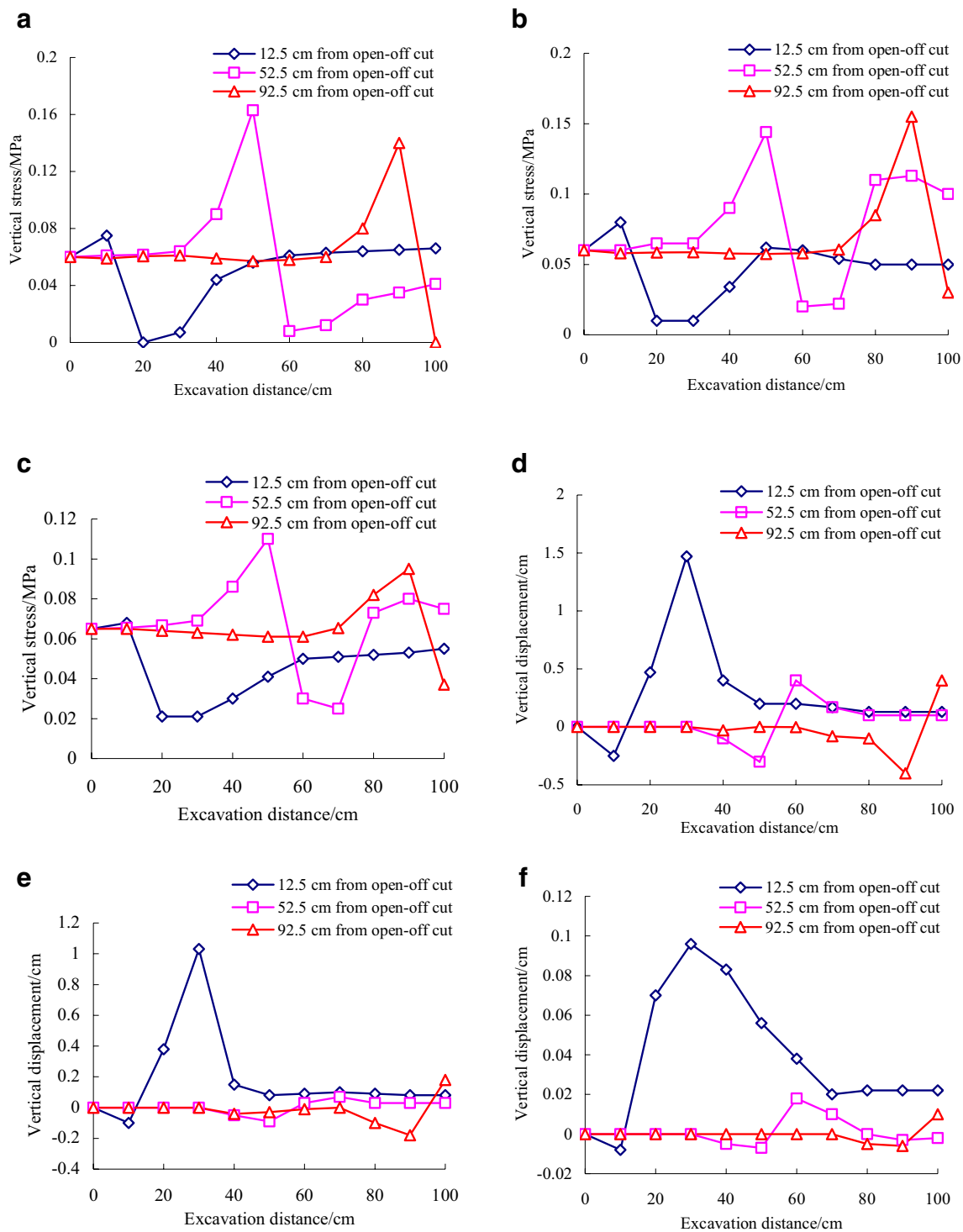


Fig. 5 Vertical stress and vertical displacement in the floor during excavation process. **a** Observation line 1, vertical stress; **b** observation line 2, vertical stress; **c** observation line 3, vertical stress; **d**

observation line 1, vertical displacement; **e** observation line 2, vertical displacement; **f** observation line 3, vertical displacement

fractures occurred. This led to water inrush through the floor before the first weighting of the roof, which will be described in detail below. The heave of the other measuring

points, which were 52.5 and 92.5 cm, respectively, from the open-off cut, were not so obvious because of periodic roof weighting. No water inrush occurred there because no

natural geologic structures, such as faults or karst collapse, existed.

Flow Rate Evolution during Excavation

Apparently, the confined water cannot penetrate through the water-resistant floor strata without the formation of a water inrush channel. As excavation distance increases, a mining-induced fractured zone develops, weakening the water resistance, and allowing pressurized water to rise up through the aquitard layer. Ultimately, a macroscopic fracture may be formed in the floor strata, hydraulically linking the confined aquifer and the void space, allowing confined water to rapidly burst into the mine.

Figure 6 displays the variations in water flow rate before and after the formation of the water inrush channels. Because the dry test materials and some non-penetrative fractures formed in the aquitard layer absorbed a certain amount of water, the flow rate was more than zero but less than 2 L/h before the excavation distance reached 30 cm. The key pathway for water outburst was formed completely when the excavation distance reached 30 cm, causing the flow rate to quickly increase to 10 L/h. A steady stream of

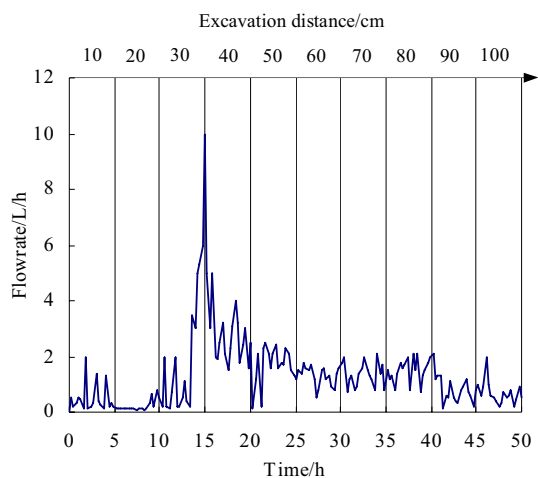
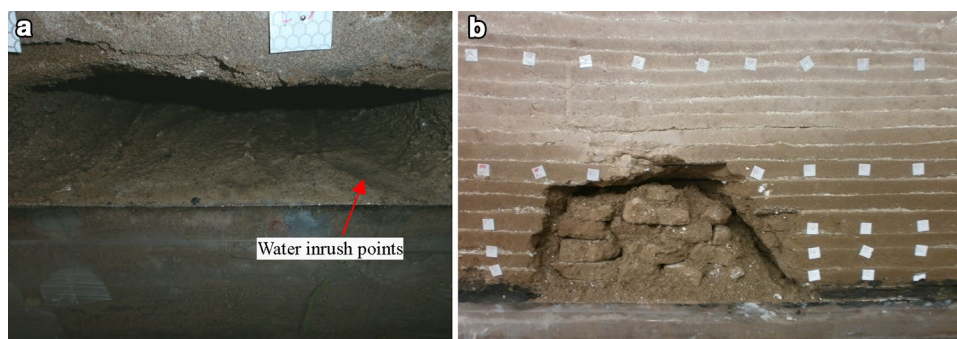


Fig. 6 Flow rate during the excavation process

Fig. 7 Water inrush from floor and first weighting of roof. **a** Water inrush phenomenon; **b** first weighting of roof



water was observed in the mining face (Fig. 7a), which corresponded to the maximum heave of the floor before the first weighting of the roof (Fig. 5d–f). However, when the excavation distance reached 35 cm, the first weighting of the roof happened (Fig. 7b), reducing the likelihood of water inrush through the floor. Actually, from Fig. 6, we can also see that the flow rate decreased overall with increasing excavation distance, so that no more water inrush events occurred. All in all, the long distance of hanging roof resulted in a large floor heave and the formation of water inrush channels before the first weighting of the roof. Thus, water inrush tended to occur in the mining face near the open-off cut.

Control Techniques

Techniques to lower the confined aquifer pressure and/or increase the aquiclude thickness could be used to avoid water inrush into the excavated space. But because the Ordovician limestone is water-rich and has a wide range of hydraulic contact with the surrounding aquifer, it is hard to control the situation using dewatering (drainage) alone. When grouting is also used to increase the aquiclude thickness, karst fissure and water-conducting fractures in the confined aquifer are filled with injected cement grout to cut off most of the water supply channels. Thus, the water-rich aquifer can be locally transformed into an aquiclude or a weak aquifer, which also helps improve the effectiveness of decreasing the confined aquifer pressure by drainage. Also, in theory at least, artificial caving can be used to shorten the first weighting distance of the roof to below the critical length, thereby preventing water inrush, though such measures were not tested in these experiments.

Conclusions

1. A water inrush physical simulation test system based on a YMD-E mining physical simulation device was designed and used to study the inrush mechanism during mining above a confined aquifer. Although differences

existed between the similar material and the actual rock, the process and phenomenon of water inrush from the underlying confined aquifer could be accurately simulated when suitable materials were used.

2. The vertical stress of the measuring point in the floor consistently increased as the mining face approached, then decreased after the face had passed, and finally returned to near its original state as the roof fell. Meanwhile the floor first compressed as the mining face approached, then heaved after the face had passed, and recompressed to a position that was a little higher than its original height as the roof fell.
3. Water inrush occurred at the open-off cut before the first weighting of the roof when the excavation distance reached 30 cm and the floor heave reached 1.47 cm. There was no further water inrush afterwards. These conclusions will be useful during mining of the simulated panel and may contribute in a general way to understanding of water inrush when mining above confined aquifers.

References

- Cheng T, Guo B, Wang L, Yang X (2016) Numerical analysis on water inrush from floor during mining above confined aquifer at Jiulishan coal mine. *Electron J Geol Eng* 21:5749–5761
- Guo B (2008) Numerical analysis on water-inrush process due to floor heave. *J Coal Sci Eng* 14:225–229
- Hu Y, Zhao Y, Yang D (2007a) Simulation theory & method of 3D solid-liquid coupling. *J Liaoning Tech Univ* 26:204–206 [Chinese]
- Hu Y, Zhao Y, Yang D (2007b) 3D solid-liquid coupling experiment study into deformation destruction of coal stope. *J Liaoning Tech Univ* 26:520–523 (Chinese)
- Huang H, Mao X, Yao B, Pu H (2012) Numerical simulation on fault water-inrush based on fluid-solid coupling theory. *J Coal Sci Eng* 18:291–296
- Li L, Qian M, Yin Y (1997) Research on the tests of water-inrush from floor simulated by similar materials. *Coal Geol Explor* 25:33–36 (Chinese)
- Li S, Xu F, Zhang Q, Li L, Wang W, Liu H (2016) Analysis and construction techniques for a water seal for underground mines subjected to water inrush. *Mine Water Environ* 35:168–179
- Sun W, Zhang S, Li Y, Lu C (2015) Development application of solid-fluid coupling similar material for floor strata and simulation test of water-inrush in deep mining. *Chin J Rock Mech Eng* 34(S1):3665–3670 [Chinese]
- Sun W, Zhou W, Jiao J (2016) Hydrogeological classification and water inrush accidents in china's coal mines. *Mine Water Environ* 35:214–220
- Wang J, Park H (2003) Coal mining above a confined aquifer. *Int J Rock Mech Min Sci* 40:537–551
- Yang Y, Li K (1997) The water inrush mechanism in coal seam floor by the physical analogy simulation technique. *Coal Geol Explor* 25:33–36 (Chinese)
- Yin H, Wei J, Lefticariu L (2016) Numerical simulation of water flow from the coal seam floor in a deep longwall mine in China. *Mine Water Environ* 35:243–252
- Zhu W, Wei C (2011) Numerical simulation on mining-induced water inrushes related to geologic structures using a damage-based hydromechanical model. *Environ Earth Sci* 62:43–54
- Zhu D, Wang C, Tong H (1999) Analogy simulation method for water invasion forecasting of mining influenced coal seam floor. *Coal Geol Explor* 27:37–43 (Chinese)